

Optimization and Simulation of Electrochemical Machining of Cooling Holes on High Temperature Nickel-Based Alloy

Mingxia Chai, Zhiyong Li*, Xuening Song, Jianhua Ren, Qingwei Cui

School of Mechanical Engineering, Shandong University of Technology, Zibo 255049, China

*E-mail: lzy761012@sdut.edu.cn

Received: 13 May 2021 / Accepted: 8 July 2021 / Published: 10 August 2021

To improve the electrochemical machining (ECM) precision and machining efficiency of aeroengine turbine blade cooling holes, taking the lateral gap and material removal rate as performance evaluation indicators, the machining accuracy and machining efficiency of ECM cooling holes as a function of the machining voltage, electrode feed rate and electrolyte concentration were explored through orthogonal experiments and single-factor experiments. The results show that among the three process parameters, the electrode feed rate is an important factor affecting the side clearance, and the processing voltage is an important factor affecting the material removal rate, which provides guidance for the optimization of ECM process parameters. Based on the cooling hole samples obtained from basic experiments, the influence of three process parameters on the distribution of the pressure field in the ECM region was analysed by computational fluid dynamics (CFD) simulations. Combined with those in the basic experiments, the optimal process parameters were obtained: machining voltage $U=10$ V, electrode feed rate $f=0.66$ mm/min, and electrolyte concentration $\zeta=11\%$.

Keywords: Cooling hole; Electrochemical machining (ECM); Computational fluid dynamics (CFD); Side clearance; Material removal rate

1. INTRODUCTION

Cooling holes are an important structure of turbine blades of high-performance aeroengines, and research on the manufacturing technology of cooling holes has been widely conducted [1, 2]. The commonly used cooling hole processing technologies include laser beam machining (LBM), electrical discharge machining (EDM), and electrochemical machining (ECM), but LBM and EDM can cause thermal damage [3, 4, 5]. ECM has become one of the important processes for machining cooling holes because of its machining process without tool wear, a recast layer and a heat affected zone [6, 7]. However, there are many factors that affect the ECM process, which can easily lead to instability of the

machining process. Therefore, improving the accuracy and efficiency of ECM of cooling holes has been a concern of researchers [8, 9]. Studies have shown that the electrode feed rate, machining voltage, electrolyte inlet pressure and electrolyte concentration all affect the diameter and taper of cooling holes [10]. The change in current density is the main factor affecting the surface quality of cooling hole machining. Low current densities yield inhomogeneous electrochemical dissolution of different microstructural areas of the material and lead to rough surfaces. High surface qualities can be achieved by employing homogenous electrochemical dissolution, which can be undertaken by high current densities [11]. Optimization of the process parameters can minimize the radial overcutting of machined holes by ECM [12], and changing the electrolyte pressure can improve the shape accuracy of holes [13]. In addition to the optimization of technological parameters, the improvement of machining technology can also effectively improve the precision and efficiency of ECM. Electrochemical discharge drilling can effectively improve the surface integrity of the holes, and there is no recast layer, no melted debris, and no residual tensile stress [14]. Zhang et al. proposed a novel hybrid machining method, i.e., tube electrode high-speed electrochemical discharge drilling, which can effectively improve the material removal rate and hole diameter. During the machining process, the recast layer generated by EDM can be effectively removed by ECM [15]. Zhu et al. demonstrated that a wedge-shaped electrode was a feasible method to improve the shape accuracy of machined holes [16].

In addition, ECM is affected by the electrolyte flow field, electric field, temperature field, etc., which is a typical multifield coupling problem, and its actual machining process is difficult to control and predict in real time. With the increasing maturity of CFD, it is helpful for researchers to determine the multifield coupling characteristics of ECM and its influence laws on ECM accuracy, efficiency and stability [17]. With the help of simulation software, an electrolyte flow mode was constructed [18], numerical simulation of the flow field in the ECM of a hollow tube electrode was carried out [19], and multifield coupling simulation was carried out to analyse the ECM process [20]. Based on this, the ECM process was optimized by combining with experiments, effectively saving experimental costs and time [21].

In this paper, the cooling holes of turbine blades of high-temperature nickel-based alloys in aeroengines were taken as the research object. Through orthogonal analysis and single factor analysis of the basic experiments on the cooling holes, the effects of machining voltage (U), electrode feed rate (f) and electrolyte concentration (ζ) on the machining accuracy and efficiency were obtained. Based on the geometric data of the cooling holes machined by ECM, a cooling hole analysis model was established, and a CFD simulation study of the pressure field distribution in the cooling hole machining gap was carried out by using the model to further explore the influence of various process parameters on the ECM process of the cooling holes.

2. EXPERIMENTAL

2.1. Processing principle and performance characterization of cooling holes

Cooling holes were processed by shaped tube electrolytic machining (STEM), and the experimental equipment is shown in Figure 1, which is mainly composed of a PC control system,

electrode feed system, electrolyte circulating filtration system and monitoring system. The PC control system can control the multi-axis position and speed of the machine tool and transmit the relevant parameters of the machine tool in real time. The feed system is servo-driven, and the electrode feed is a closed loop controlled by a grating ruler with a resolution of 1 μm . The electrolyte circulation filtration system adopts a high-pressure diaphragm pump to realize the circulating flow of electrolyte. The monitoring system uses a data acquisition card to monitor the parameters of the ECM process.

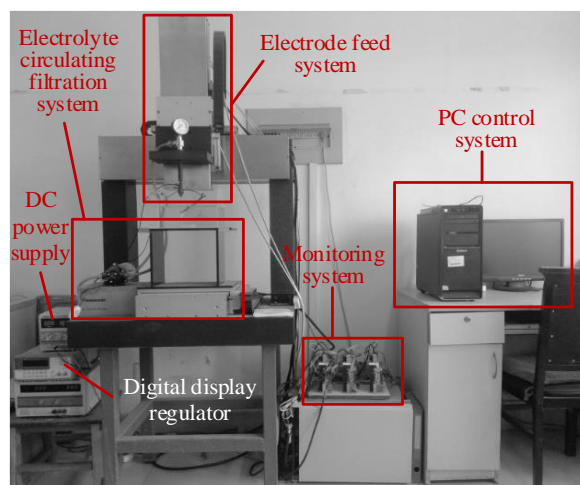


Figure 1. Experimental setup of the STEM process

Figure 2 is the schematic diagram of the cooling holes in STEM. During processing, the electrolyte flows through the inner hollow part of the tube electrode, removing the electrical corrosion products and heating in time to ensure the stability of the process. The cathode was a brass tube electrode with a diameter of 0.8 mm and an inner diameter of 0.3 mm. The side of the cathode was insulated with epoxy resin, and the thickness of the insulation layer was 50 μm . 0.2 mm of the processing end face was reserved without insulation treatment. The workpiece is made of an Inconel 718 sheet with a thickness of 1.7 mm. The Ni content is between 50~55%, and the other elements are Cr, Nb, Mn, Ti, etc. The angle between the cooling hole and blade surface of the aeroengine turbine blade is mostly 15°~60°. In this study, all workpieces are installed at 45° with respect to the horizontal surface, and the depth of the machining hole is 2.4 mm. The electrolyte composition is a NaNO_3 solution, which has high machining accuracy, weak corrosion and low processing cost.

In ECM, the lateral gap is usually used to characterize ECM accuracy [22]. Under normal processing conditions, the smaller the lateral gap is, the higher the formation accuracy of cooling holes [23]. In this experiment, a German Axio-Lab.A1 metallographic microscope was used to detect the surface morphology of the cooling holes, and the formula of the lateral gap Δs is as follows:

$$\Delta s = \frac{D-d}{2} \quad (1)$$

where D is the diameter of the cooling holes (μm) and d is the tube electrode diameter (μm).

The machining efficiency was characterized by the material machining removal rate MRR :

$$MRR = \frac{m_1 - m_2}{\rho t} \tag{2}$$

where m_1 and m_2 are the mass of the workpiece before and after ECM, respectively (g), ρ is the density of the high-temperature nickel-based alloy Inconel 718 (8.24 g/cm³), and T is the ECM experiment time (min).

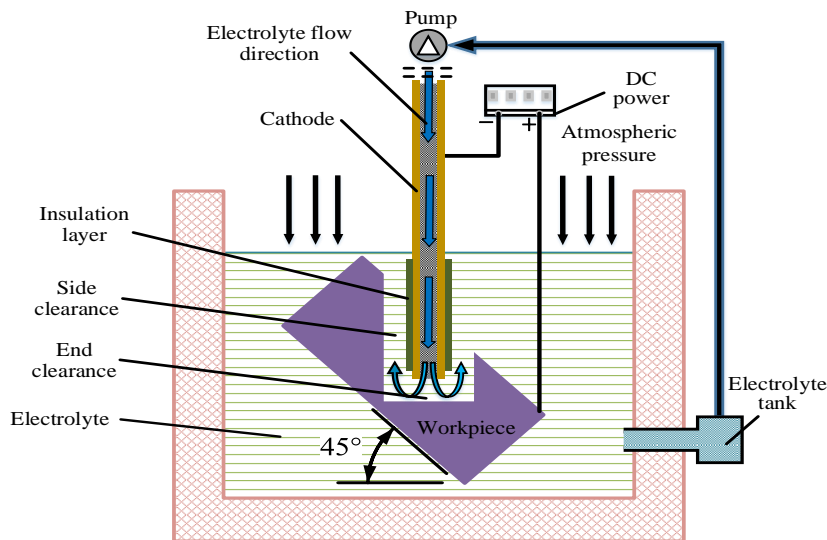


Figure 2. The schematic diagram of STEM

2.2. Orthogonal experiment and single factor experiment plan

The influences of machining voltage, electrode feed rate and electrolyte concentration on the machining accuracy and efficiency of the cooling holes in STEM were studied by orthogonal experiments with three factors and three levels. The selected process parameters and levels are shown in Table 1. The process parameters are combined according to orthogonal table L₉ (3⁴). Three tests were carried out under each set of processing parameters, the corresponding lateral gap and material machining removal rate were measured, and the average values were calculated. The scheme and the measurement results are shown in Table 2.

In the analysis of orthogonal experiment results, the magnitude of the range value R reflects the degree of influence of the change in the selection level of the corresponding factor on the index. The range value can be calculated as:

$$R_j = \max(K_{ij}) - \min(K_{ij}) \tag{3}$$

where i represents the factor levels from 1 to 3; j is the process parameters of machining voltage, electrode feed rate, and electrolyte concentration; R_j denotes the range value of factor j ; and K_{ij} indicates the mean value of the corresponding indices of factor j at all level i . The larger the value of R is, the greater the influence degree, and vice versa.

Based on the analysis results obtained from the orthogonal experiment to further optimize the process parameter, a single factor experiment was used to analyse the influence of each process

parameter on the lateral gap and material machining removal rate, and the specific parameters were designed according to the orthogonal experiment results.

Table 1. Factor level table of orthogonal experiment for machining cooling holes

Factors	Machining voltage(V)	Electrode feed rate (mm/min)	Electrolyte concentration (wt%)
Level 1	8	0.42	7
Level 2	10	0.54	9
Level 3	12	0.66	11

Table 2. The design and results of orthogonal experiment of machining cooling holes

No.	Machining voltage (V)	Electrode feed rate (mm/min)	Electrolyte concentration (wt%)	Lateral gap (μm)	Material removal rate (mm^3/min)
1	8	0.42	7	134.91	0.353
2	8	0.54	9	109.75	0.449
3	8	0.66	11	105.34	0.511
4	10	0.42	9	121.16	0.487
5	10	0.54	11	119.87	0.519
6	10	0.66	7	98.32	0.531
7	12	0.42	11	131.63	0.518
8	12	0.54	7	129.72	0.587
9	12	0.66	9	123.84	0.614

2.3. Establishment of the simulation model

The electrolyte pressure distribution in the processing area is analysed by the standard k- ϵ turbulence model. The following assumptions of the pressure field of electrochemical machining are made:

- (1) The electrolyte flow is incompressible and a constant Newtonian flow.
- (2) The energy dissipation caused by the change in the medium temperature in the machining process is negligible [24].
- (3) The electrolyte flow is constrained by the mass conservation equation and momentum conservation equation [25].

The standard k- ϵ turbulence model is described by equation [26]:

$$\begin{aligned} \frac{\partial(\rho k u_i)}{\partial x_i} &= \frac{\partial}{\partial x_j} \left[\left(\mu + \frac{\mu_t}{\sigma_k} \right) \frac{\partial k}{\partial x_j} \right] + G_k - \rho \varepsilon \\ \frac{\partial(\rho \varepsilon u_i)}{\partial x_i} &= \frac{\partial}{\partial x_j} \left[\left(\mu + \frac{\mu_t}{\sigma_\varepsilon} \right) \frac{\partial \varepsilon}{\partial x_j} \right] + \frac{C_{1\varepsilon} \varepsilon}{k} G_k - C_{2\varepsilon} \rho \frac{\varepsilon^2}{k} \\ \mu_t &= \rho C_\mu \frac{k^2}{\varepsilon} \end{aligned} \tag{4}$$

where u_i is the time-averaged velocity, μ_t is the turbulent viscosity, k is the turbulent kinetic energy, ε is the dissipation rate of turbulent kinetic energy, and G_k is the generation of turbulent kinetic energy caused by the average velocity gradient. C_μ , $C_{1\varepsilon}$, $C_{2\varepsilon}$, σ_k and σ_ε are model constants, and $C_\mu=0.09$, $C_{1\varepsilon}=1.44$, $C_{2\varepsilon}=1.92$, $\sigma_k=1.00$, and $\sigma_\varepsilon=1.30$, respectively.

According to the section shown in Figure 3, the cooling hole sample was cut three times on a DMU 70 Evolution CNC machine tool with a depth of 0.425 mm each time to obtain sections 2, 3 and 4, and its surface morphology is shown in Figure 4. The geometric contour dimensions of the above five sectional faces were collected to establish a two-dimensional geometric model, as shown in Figure 5. The workpiece and cathode were represented by the workpiece contour and the cathode contour, respectively.

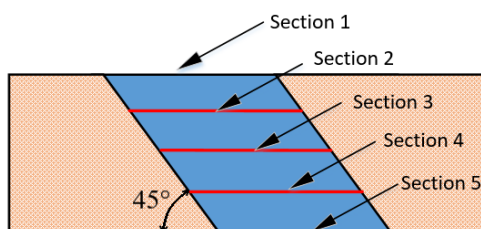


Figure 3. Measured sections of the cooling holes sample

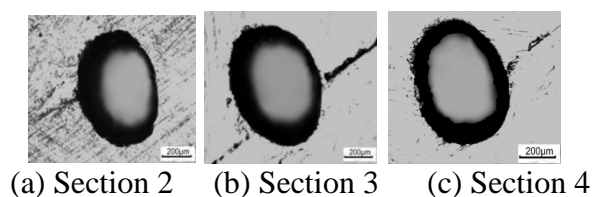


Figure 4. Milled sections of a machined cooling hole samples

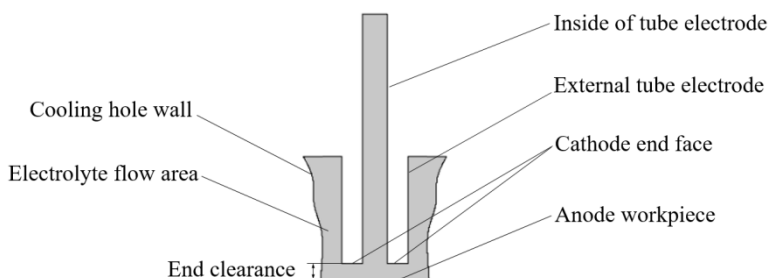


Figure 5. Two-dimensional model of film cooling hole runner

3. RESULTS AND DISCUSSION

3.1. Orthogonal experiment analysis

Table 3. Range analysis table of the lateral gap

Levels	Machining voltage	Electrode feed rate	Electrolyte concentration
K_1	116.667	129.233	120.983
K_2	113.117	119.780	118.250
K_3	128.397	109.167	118.947
R	15.280	20.066	2.733

Table 4. Range analysis table of material removal rate

Levels	Machining voltage	Electrode feed rate	Electrolyte concentration
K_1	0.438	0.453	0.490
K_2	0.512	0.518	0.517
K_3	0.573	0.552	0.516
R	0.135	0.099	0.027

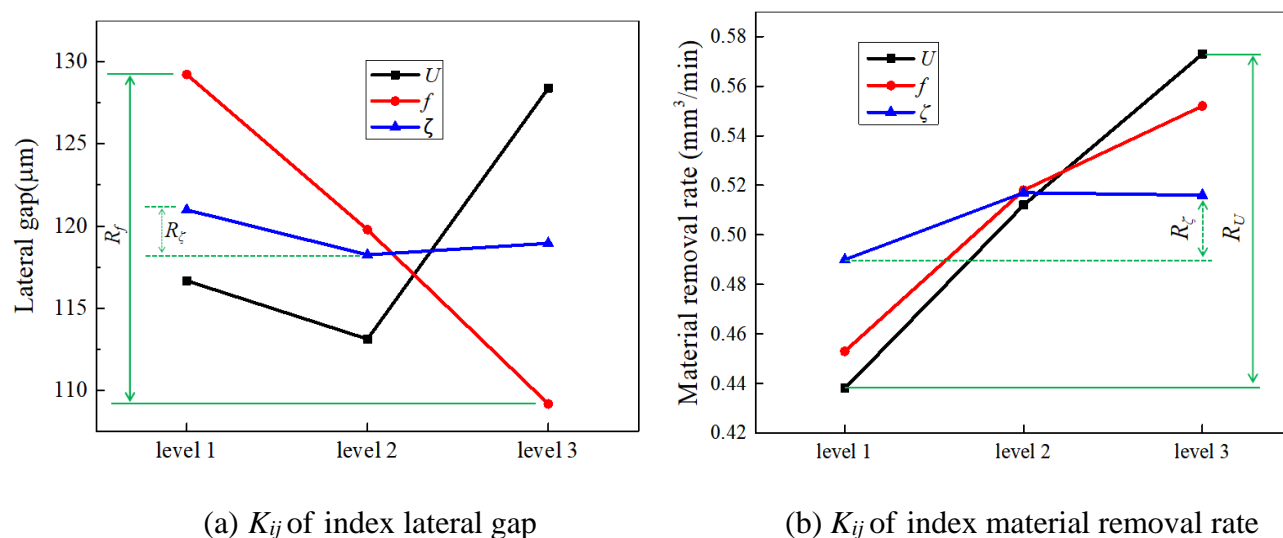


Figure 6. Various trends in the mean values of two indices under different factor levels

The results of the range analysis of the lateral gap and material removal rate are listed in Tables 3 and 4, respectively. According to this, the variation trend of the mean value of the two indicators at different factor levels is obtained, as illustrated in Figure 6. By comparing the range value, the order of the influence degree of the three process parameters on the side clearance is electrode feed rate >

machining voltage > electrolyte concentration, and the order of the influence degree for the material machining removal rate is machining voltage > electrode feed rate > electrolyte concentration. According to K_{ij} , the optimal processing parameters under each factor can be obtained, and then the optimal process parameter combination can be obtained. The higher the value of K_{ij} is, the lower the machining accuracy and the higher the machining efficiency. Therefore, the best process parameter combination to improve the cooling hole formation accuracy is $U_2f_3\zeta_2$, that is, machining voltage $U=10$ V, electrode feed rate $f=0.66$ mm/min, and electrolyte concentration $\zeta=9\%$. The optimum process parameters were $U_3f_3\zeta_2$, that is, machining voltage $U=12$ V, electrode feed rate $f=0.66$ mm/min, and electrolyte concentration $\zeta=9\%$.

3.2. Single factor experiment analysis

3.2.1. Influence of machining voltage on the lateral gap and material machining removal rate

According to the orthogonal test, better cooling hole formation accuracy can be obtained when the machining voltage is 10 V, and a higher material machining removal rate can be obtained when the machining voltage is 12 V. Therefore, the influence of the machining voltage ($U=6$ V, 8 V, 10 V, 12 V, and 14 V) on the lateral gap and material machining removal rate was investigated with the electrode feed rate $f=0.66$ mm/min and electrolyte concentration $\zeta=9\%$ unchanged. The experimental results are shown in Figure 7. With increasing processing voltage, the lateral gap and material machining removal rate both increase. When the machining voltage increases from 6 V to 14 V, the material removal rate increases from 0.432 mm³/min to 0.657 mm³/min, and the machining efficiency increases by 52.08%, but the lateral gap increases from 75.39 μm to 153.45 μm , the surface roundness of the cooling hole worsens and the taper obviously increases. Under the premise of ensuring processing accuracy, the processing voltage should not be too large, and a machining voltage $U=10$ V is appropriate.

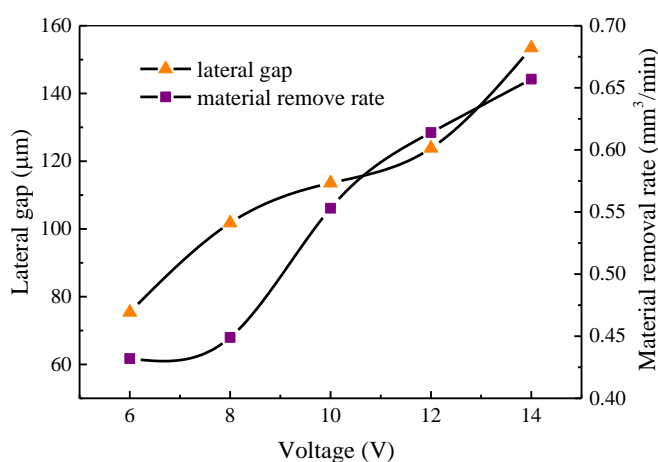


Figure 7. Variation of lateral gap and material machining removal rate with voltage

3.2.2. Influence of electrode feed rate on the lateral gap and material machining removal rate

Through single factor analysis of machining voltage and the orthogonal experiment, machining voltage $U=10$ V and electrolyte concentration $\zeta=9\%$ were selected to study the influence of electrode feed rate ($f=0.30$ mm/min, 0.42 mm/min, 0.54 mm/min, 0.66 mm/min, and 0.78 mm/min) on the machining accuracy and efficiency of cooling holes. According to the analysis of the experimental results in Figure 8, the lateral gap is negatively correlated with the feed speed, and the material machining removal rate is positively correlated with the feed speed. When the electrode feed rate $f=0.66$ mm/min, both high machining accuracy and high machining efficiency can be guaranteed, which is an appropriate process parameter choice. However, the feed speed cannot be increased continuously. When the electrode feed rate $f=0.78$ mm/min, the anode dissolution speed is less than the electrode feed rate, and there are several short circuits in the experiment, serious burns on the surface of cooling holes, and "blind holes" in the processing. Therefore, on the premise of ensuring the match between the normal dissolution speed of the workpiece and the feed speed of the tool, it is very important to appropriately increase the electrode feed rate to improve the machining accuracy and efficiency of the cooling hole.

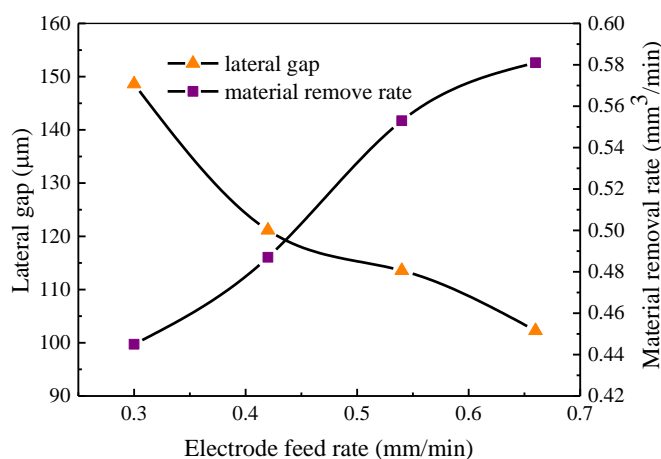


Figure 8. Variation of lateral gap and material machining removal rate with feed rate

3.2.3. Effect of electrolyte concentration on the lateral gap and material machining removal rate

Under the condition of machining voltage $U=10$ V and electrode feed rate $f=0.66$ mm/min, the lateral gap of the cooling holes and the material machining removal rate varied with the electrolyte concentration ($\zeta=5\%$, 7%, 9%, 11%, 13%, and 15%) as follows: both increased with the increase of electrolyte concentration (as shown in Figure 9). This is mainly because the increase in solution concentration causes an increase in conductivity, electron transfer speed, current density and electrochemical removal ability, so the processing efficiency is improved, but the lateral gap is increased and the machining accuracy is reduced. Therefore, to ensure machining accuracy, the concentration of electrolyte should not be too high, and electrolyte concentration $\zeta=11\%$ is considered to be the best, which can meet both high machining accuracy and machining efficiency.

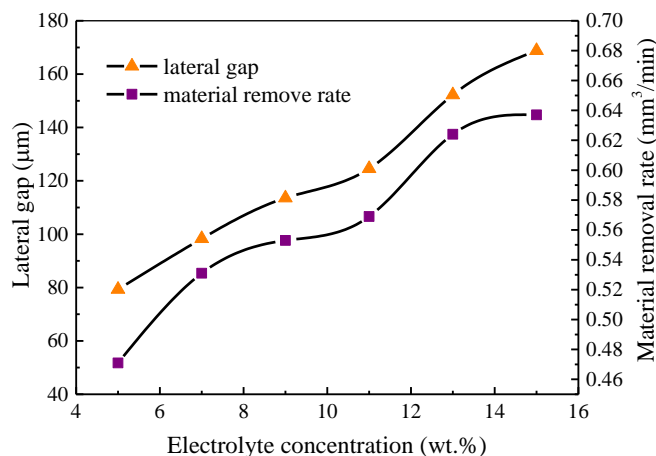


Figure 9. Variation of lateral gap and material machining removal rate with electrolyte concentration

3.3. Simulation and analysis of the pressure field in the distance between electrode

3.3.1. Influence of machining voltage on the pressure distribution in the machining area

Figure 10 shows the simulation analysis diagram of the pressure distribution in the processing area under different processing voltages. As seen from the figure analysis, the pressure in the ECM area of the tube electrode is distributed symmetrically on the whole, which can effectively avoid the sloshing of the electrode caused by the different pressures on both sides of the wall and is conducive to the stability of ECM. However, three groups under the condition of voltage occurred on the processing area of the negative pressure zone (blue area). The negative pressure region will make bubbles in the electrolyte when the pressure is lower than the air separation pressure, which leads to separation in the solution, causing air bubbles and affecting the continuity and uniformity of the flow field. This not only reduces the machining accuracy but also increases the risk of short circuits.

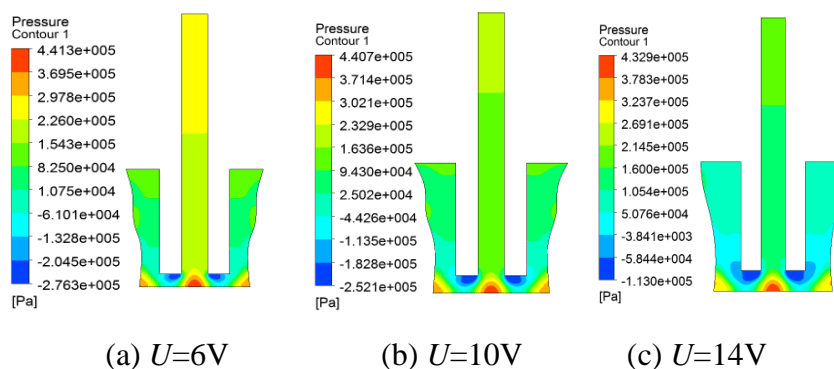


Figure 10. Pressure distribution under different voltage

Compared with Figure 10 (a) ~ (c), when the machining voltage increases from $U=6$ V to $U=10$ V, the absolute value of the maximum pressure in the negative pressure area decreases from 2.763×10^5 Pa to 2.521×10^5 Pa, which is conducive to the improvement of the processing stability. However, when

the machining voltage continues to increase to 14 V, although the highest pressure value in the negative pressure area decreases, the negative pressure area diffuses from the bottom clearance to the side clearance, and the influence area expands, which can easily disturb the flow stability of the electrolyte and reduce the machining accuracy. When the machining voltage $U=10$ V, a better processing effect can be obtained, which is consistent with the basic experiment.

3.3.2. Influence of electrode feed rate on the pressure distribution in the machining area

According to Figure 11, with increasing electrode feed rate, the pressure inside the tube electrode increases continuously (1.648×10^5 Pa- 2.463×10^5 Pa- 3.076×10^5 Pa). Although the absolute value of the maximum pressure in the negative pressure area does not change much (2.198×10^5 Pa- 2.002×10^5 Pa- 2.195×10^5 Pa), the affected area continues to decrease. Therefore, under the condition of high pressure, the negative pressure area in the bottom gap decreases, and the gas content in the solution decreases, which improves the integrity and continuity of the flow field. At the same time, the pressure in the tube electrode increases, which promotes the mobility of the electrolyte and can remove the electrolytic products in time, which is conducive to the stability of ECM. Therefore, a better processing effect can be obtained under the condition of an electrode feed rate $f=0.66$ mm/min.

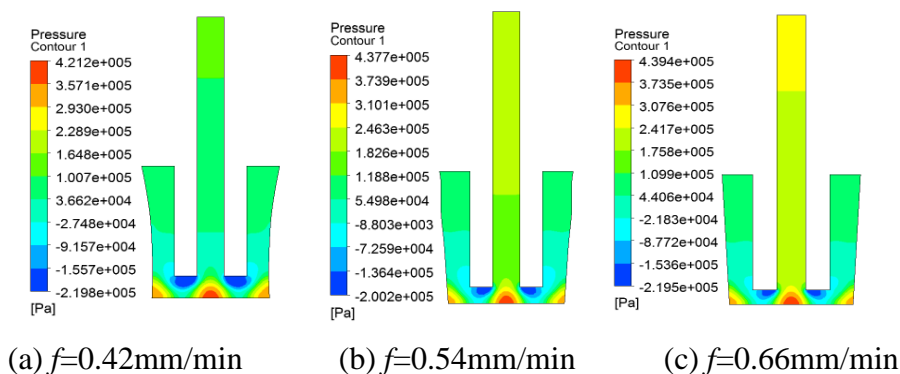


Figure 11. Pressure distribution under different feed rate

3.3.3. Effect of electrolyte concentration on the pressure distribution in the machining area

As shown in Figure 12, with increasing electrolyte concentration, the absolute value of the pressure in the blue negative pressure zone in the machining gap continues to decrease, but the distribution area continues to increase. However, with increasing electrolyte concentration, the rate of electrolytic reaction is accelerated, the number of electrolytic products per unit time increases, and gas generation increases. The low pressure area will cause the gas to be easily separated from the solution, forming cavitation, which is not conducive to the processing stability, and the expansion of the negative pressure area will affect the side clearance, so the electrolyte concentration should not be too large. To ensure both a small absolute negative pressure and a small negative pressure area, electrolyte concentration $\zeta=11\%$ is the preferred processing parameter.

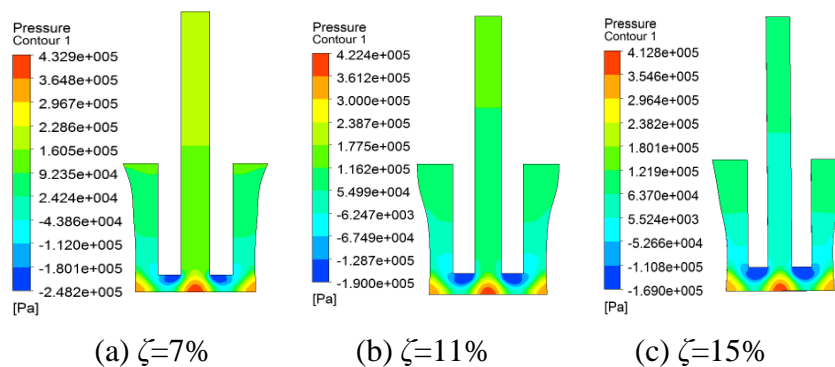
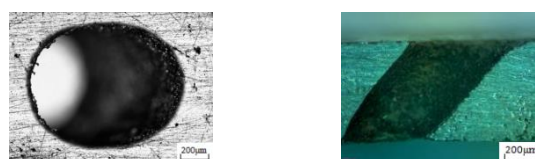


Figure 12. Pressure distribution under different electrolyte concentrations

3.4. Cooling hole experiment verification

Through the orthogonal experiment, single factor experiment and CFD pressure field analysis, in order to improve the ECM stability, ECM precision and ECM efficiency, the process parameters should choose a moderate processing voltage and electrolyte concentration with a high electrode feed rate, and the optimal process parameter combination was determined as machining voltage $U=10$ V, electrode feed rate $f=0.66$ mm/min and electrolyte concentration $\zeta=11\%$. The lateral gap of the cooling hole under this process parameter is $84.27 \mu\text{m}$, and the material removal rate is $0.613 \text{ mm}^3/\text{min}$. This can obtain a stable machining process, high hole formation accuracy, and good surface morphology. Figure 13 (a) shows the microscopic morphology of the cooling hole, and (b) shows its section.



(a) Microscopic morphology of cooling hole (b) Cooling hole section view

Figure 13. Topography of ECM Cooling Hole under the Optimal Combination of Process Parameters

3.5. Comparison with similar results

Electrochemical machining of air film cooling holes in aeroengines has various forms, but each has its own advantages and disadvantages. The electrochemical discharge drilling machining speed is much higher than the speed of electrochemical drilling. However, the machining accuracy requires a high processing time, and stray current easily causes stray corrosion and destroys the surface integrity of the workpiece [27]. In electrochemical drilling, the hole exit accuracy is very sensitive to the electrode feeding depth and easily results in stray removal at the hole exit and an etched and pitted surface [28, 29]. Mechanical microdrilling has higher requirements on the tool, and the tool life is significantly

reduced when drilling inclined holes [30]. Tube electrode high-speed electrochemical discharge drilling could facilitate the removal of machining byproducts, but the processing cost is higher [31]. Shaped tube electrolytic machining is an attractive process for drilling deep holes in superalloys with diameters less than 1.0 mm and aspect ratios up to 300. It is versatile and has a relatively low cost [32]. The specific comparisons are shown in Table 5.

Table 5. Comparison of similar discussion and results

No.	Methods	Research object	Electrolyte	Machining effect	Ref.
1	Electrochemical discharge drilling	nickel-based superalloy	NaNO ₃ solution	The machining speed of ECDD can reach 130 μm/s. The surface of the machining hole is smooth, there is no recasting layer, and there are only a few defects.	27
2	Electrochemical drilling	Inconel 718	100 g/L NaNO ₃ + 100 g/L NaCl	The method can minimize the stray removal of material at the hole exit in ECD to enhance the exit accuracy. The ratios of stray removal in the diameter at the hole exit can remain less than 0.1.	28
3	Electrochemical drilling	Inconel 718	NaNO ₃ solution	Under the condition of a constant flow of 210 ml/min and feed rate of 2.0 mm/min, the roundness error of ECD is 18.19 μm.	29
4	Mechanical micro-drilling	Inconel 718	N.A.	This method easily causes tool wear, and the cutting edge coating easily peels off. It is affected by radial force, the aperture is irregular, and the deviation is large. As the number of drilled holes increases, different types of surface alterations are observed on the drilled surfaces.	30
5	Tube electrode high-speed electrochemical discharge drilling	Nickel-based superalloys	N.A.	As the inner diameter of the tube electrode increases, the lateral gap first decreases and then increases, with the minimum lateral gap at 250 μm.	31
6	Shaped tube electrolytic machining	Inconel 718	NaNO ₃ solution	The lateral gap of the cooling hole under this process parameter is 84.27 μm, and the material removal rate is 0.613 mm ³ /min.	This work

4. CONCLUSIONS

1) An orthogonal experiment shows that the order of influence of the three process parameters on the ECM accuracy is as follows: electrode feed rate > machining voltage > electrolyte concentration.

The order of influence on the processing efficiency is as follows: machining voltage > electrode feed rate > electrolyte concentration.

2) Combining basic experiments and CFD simulation analysis, the change in process parameters will cause changes in the pressure field in the processing area, resulting in gas-liquid two-phase changes and affecting the stability of electrochemical machining. The study has shown that a moderate processing voltage and concentration of electrolyte with a larger electrode feed rate can satisfy the electrochemical machining precision and efficiency of cooling holes.

3) Comprehensive analysis shows a good surface integrity of the cooling hole and high processing efficiency when machining voltage $U=10$ V, electrode feed rate $f=0.66$ mm/min and electrolyte concentration $\zeta=11\%$ are combined.

ACKNOWLEDGEMENTS

This project was supported by National Nature Science Foundation of China (No.51805302) and Shandong Provincial Natural Science Foundation of China -“Dynamic Mechanism of 3D Flow Field and Basic Experimental Study on Electrochemical Machining Cooling Hole of High Temperature Nickel-based Alloy Blade”(ZR2014EEM038)

References

1. J. Z. Zhang, S. C. Zhang, C. H. Wang, and X.M Tan, *Chin. J. Aeronaut.*, 33 (2020) 1119.
2. S. Peetermans, and E. H. Lehmann, *NDT & E Int.*, 79 (2016) 109.
3. Z. Y. Li, X. T Wei, and Y. B. Guo, *Machining Science and Technology: An International Journal*, 19 (2015) 361.
4. S. K. Amineh, A. F. Tehrani, and A. Mohammadi, *Int. J. Adv. Manuf. Technol.*, 66 (2013) 1793.
5. H. Jonas, B. Jonan, W. Anders, and B. Tomas, *Int. J. Adv. Manuf. Technol.*, 100 (2019) 1575.
6. J. S. Zhao, F. Y. Wang, and J. W. Xu, *Acta Aeronautica et Astronautica Sinica*, 34 (2013) 2841.
7. K. P. Rajurkar, M. M. Sundaram, and A. P. Malshe, *Procedia CIRP*, 6 (2013) 13.
8. D. Zhu, Z. Z. Gu, T. Y. Xue, and A. Liu, *Chin. J. Aeronaut.*, 30 (2017) 1624.
9. G. Q. Wang, H. S. Li, N. S. Qu, and D. Zhu, *J. Mater. Process. Technol.*, 234 (2016) 95.
10. S. Ali, S. Hinduja, J. Atkinson, and M. Pandya, *CIRP Annals-Manufacturing Technology*, 58 (2009) 185.
11. M. Burger, L. Koll, E. A Werner, and A. Platz, *J. Manuf. Processes*, 14 (2012) 62.
12. W. Wang, D. Zhu, N.S. Qu, S. F. Huang, and X. L. Fang, *J. Mater. Process. Technol.*, 210 (2010) 238.
13. G. D. Liu, Y. Li, Q. C. Kong, and L. Q. Yu, *Procedia CIRP*, 68 (2018) 420.
14. C. X. Zhang, Z. Y. Xu, X. Y. Zhang, and J. Y. Zhang, *CIRP Annal-Manufacturing Technology*, 31(2020) 643.
15. Y. Zhang, Z. Y. Xu, D. Zhu, and J.Xing, *International Journal of Electrical Machining*, 92 (2015) 10.
16. D. Zhu, W. Wang, X. L. Fang, N. S. Qu, and Z. Y. Xu, *CIRP Annal-Manufacturing Technology*, 59 (2010) 239.
17. J. A. Mcgeough, P. T. Pajak, A. K. M. Desilva, and D.K. Harrison, *International Journal of Electrical Machining*, 8 (2003) 1.
18. Y. L. Chen, X. C. Zhou, P. X. Chen, and Z. Q. Wang, *Chin. J. Aeronaut.*, 33 (2020) 1057.
19. G. D. Liu, Y. Li, Q. C. KONG, and L. Q. Yu, *Procedia CIRP*, 6 (2018) 420.
20. K. Jerzy, and Z. K. Maeia, *Procedia CIRP*, 4 (2016) 101.

21. F. Yang, T. Y. Ren, H. B. Wang B. X. Liu, and M. Chen, *Int. J. Adv. Manuf. Technol.*, 89 (2017) 1317.
22. J. C. Bai, J. C. Liu, Y. F. Guo, and X. D. Yang, *Mechanical Industry Press*, (2013) Beijing, Chinese.
23. J. S. Zhao, F. Wang, X. L. Zhang, Z. W. Yang, and Y. M. Lv, *Procedia CIRP*, 68 (2018) 684.
24. X. Q. Fu, M. Kang, Y. Yang, and Z. X. Liu, *China Mech. Eng.*, 24 (2013) 1038.
25. Y. L. Chen, M. Fang, D. Pei, and W. J. Wei, *China Mech. Eng.*, 27 (2016) 3087.
26. F. J. Wang, *Tsinghua University Press*, (2004) Beijing, Chinese.
27. X. Zhang, Z. Y. Xu, X. Y. Zhang and J. Y. Zhang, *CIRP Journal of Manufacturing Science and Technology*, 31 (2020) 643.
28. C. X. L. Fang, N. S. Qu, Y. D. Zhang, Z. Y. Xu and D. Zhu, *J. Mater. Process. Technol.*, 214 (2014) 556.
29. X. D. Wang, N. S. Qu, X. L. Fang, H. S. Li, *J. Mater. Process. Technol.*, 238 (2016) 1.
30. A.N. Khadtarea, R. S. Pawadea, S. Joshi, *Precis. Eng.*, 66 (2020) 166.
31. Y. Zhang, Z. Y. Xu, J. Xing, D. Zhu, *Chin. J. Aeronaut.*, 29 (2016) 1103.
32. Z. Y. Li, X. T. Wei, Y. B. Guo and M. P. Sealy, *Mach. Sci. Technol.*, 19 (2015) 361.

© 2021 The Authors. Published by ESG (www.electrochemsci.org). This article is an open access article distributed under the terms and conditions of the Creative Commons Attribution license (<http://creativecommons.org/licenses/by/4.0/>).